Novel Structure Change in Nonequimolar Complexes of Linear Poly(ethylenimine) and Octadecanoic Acid: Effects of Composition

Biye Ren, Zhiyu Cheng, Zhen Tong,* Xinxing Liu, Chaoyang Wang, and Fang Zeng

Research Institute of Materials Science, South China University of Technology, Guangzhou 510640, China

Received March 28, 2005; Revised Manuscript Received April 29, 2005

ABSTRACT: Polymer−amphiphile complexes based on specific noncovalent interactions have received considerable attention in recent years due to its simple preparation and interesting properties. However, little attention has been paid to the complex composition effect on the crystal and mesomorphous structure of amphiphile side chains in nonequimolar polymer−amphiphile complexes. The structure of a series of nonequimolar linear poly(ethylenimine)−octadecanoic acid complexes, *l*PEI−OA-*x*, with the molar ratio *x* of OA to the *l*PEI amino group ranging from 0.66 to 1.45, was investigated with WAXD, SAXS, FTIR, DSC, fluorescence spectrum, and polarized optical microscope. Two crystalline modifications β_O (β-orthorhombic) and β_T (β-triclinic) of OA side chains have been found to coexist in the complexes varying with *x*, and only 8−10 CH_2 groups in an OA molecule participate in the crystallization. The crystalline OA tails with amorphous *l*PEI form the lamella stacking structure. The complexes of $x > 1.0$ are predominant with β_O form and stacked into an end-to-end bilayer lamella with the long period of ∼5.6 nm. While for the complexes of $x < 1.0$, the β_T form is dominantly stacked in the interdigitating monolayer structure with the long period of ∼2.8 nm. The fluorescence emission from pyrene-doped complexes indicates a decrease in the microenvironment polarity with increasing *x*. The thermotropic liquid crystal state has been observed from the complexes of $x < 1.0$ at temperatures above the melting point of the OA tail crystal. This study demonstrates that the crystalline and mesomorphous structures of polyelectrolyte−amphiphile complexes can be effectively tuned by changing the relative amount of bound amphiphiles. In other words, the stacking structure of amphiphile molecules depends on the amount of added binding polyelectrolytes.

Introduction

Polymer−amphiphile complexes are attracting substantial attention in recent years due to the facility in preparing supramolecular mesomorphous structures and attaining special functions, such as low surface energy, optical, photoelectrical, drug and gene delivery, etc.[1−3] The self-assembled supramolecular structure can be constructed through specific noncovalent interactions, such as hydrogen bonding, charge transfer, ionic interactions, or coordination complexation between polymers and amphiphiles.[4,5] Both nanostructures and physicochemical properties can be delicately adjusted by the nature of both polymers and amphiphiles, such as polar groups, alkyl side chains, and volume ratio of hydrophobic to hydrophilic moieties.[1−7] Hence, the complexation of polymers with amphiphiles promises a simple and feasible way to construct various order nanostructures with special applications and also provides profound insights into the role of various noncovalent interactions in an order structure formation.

Branched poly(ethylenimine) (*b*PEI), a water-soluble polymer, has wide applications in the medical and paper industries and also is usually used as a polyelectrolyte for construction of Langmuir−Blodgett monolayer or multilayer films with various *n*-alkanoic acids or proton-donating amphiphiles in solutions.[8] Characteristic mesomorphous lamellar structures have also been reported for the complexes of *b*PEI and *n*-alkanoic acids.[9,10] It was found that the lamella long period of the complex, tendency of side chains to crystallize, and crystalline degree of side chains depended mainly on the tail length of the bound *n*-alkanoic acids. The majority of the above-mentioned investigations, however, were based on the complexes of 1:1 stoichiometry for polyelectrolytes and amphiphiles with respect to the charge sites, and little was reported on the effects of the complex composition on the structure of the packing of side chains in nonequimolar polymer−amphiphile complexes.

Recently, we prepared *b*PEI−perfluorooctanoic acid (PFOA) complexes with different compositions using the "starving addition" method, and the complex showed the critical surface tension even lower than that of poly(tetrafluoroethylene).[11] Two mesomorphous structures of interdigitating monolayer and end-to-end bilayer for the bound PFOA tail alignment with different long periods have been found to coexist in the complex and the predominant structure rests upon the molar ratio of PFOA to the amino groups of *b*PEI, which in turn determines the surface and thermal properties of the complex. This end-to-end bilayer is quite similar in structure to the lipid bilayer in the cell membrane, where the polymer behaves as the actin-based membrane skeleton and the bound aliphatic chains as the anchored protein in forming the compartment picket in the cell membrane.[12,13] Consequently, it is possible to observe the hopping diffusion in this complex, simulating the lateral movement in the cell membrane. Thus, the fabrication and active control of the delicate supramolecular structure are necessary. Nonequimolar polymer−amphiphile complexes seem to be a more facile way to understand the formation mechanism of the supramolecular structure compared with usual 1:1 stoichiometric polymer−amphiphile complexes from a viewpoint of intermolecular interactions. However, *b*PEI is a completely random, highly branched polymer con-

* Corresponding author: Tel/Fax +86-20-8711-2886; e-mail mcztong@scut.edu.cn.

10.1021/ma050647+ CCC: $30.25
Published on Web 05/27/2005

Table 1. Composition and Thermal Properties of *l*PEI−OA Complexes

sample	N (wt %)	x	T_m (°C)[a]	ΔH_m (J/g)	X_c^{OA} (%)	n_c
*l*PEI−OA-0.66	6.08	0.66	58.1	75.7	48.0	8.2
*l*PEI−OA-0.88	4.79	0.88	58.7	80.2	48.4	8.2
*l*PEI−OA-1.09	3.96	1.09	58.2, 63.4	87.1	51.1	8.7
*l*PEI−OA-1.37	3.23	1.37	57.5, 66.2	94.5	54.1	9.2
*l*PEI−OA-1.45	3.08	1.45	56.1, 67.3	100.8	57.4	9.8

[a] Peak values of Figure 7.

taining primary, secondary, and tertiary amino groups with different relative basicities; hence, linear poly(ethylenimine) (*l*PEI) may be a better alternative for fabrication of the delicate supramolecular structure of polymer−amphiphile complexes. To our knowledge, no study on the packing and crystalline structure of the nonequimolar *l*PEI−amphiphile complex has been reported up to now.

In the present paper, several complexes of *l*PEI−octadecanoic acid (OA), *l*PEI−OA-*x*, with the actual molar ratio *x* of OA to the amino group in *l*PEI ranging from 0.66 to 1.45, have been investigated with wide-angle X-ray diffraction (WAXD), small-angle X-ray scatting (SAXS), thermogravimetry analysis (TGA), differential scanning calorimetry (DSC), steady-state fluorescence spectra, and polarized optical microscope. The main goal is to experimentally illustrate the effect of the complex composition on the ordered mesomorphous, side-chain crystal and liquid crystal structure of the present complex and the possibility of controlling the supramolecular structure of the complex by simply changing the relative amount of bound amphiphiles.

Experimental Section

Complex Preparation. *l*PEI (Alfa, MW 25 000) and octadecanoic acid (OA, Shanghai Chemical Reagent Co.) were used as received. Other reagents were all commercially available. The complex (*l*PEI−OA-*x*) was prepared by mixing octadecanoic acid and *l*PEI in ethanol solution at about 75 °C just below its boiling temperature under reflux. A general procedure is as follows: 2.84 g of OA was dissolved in 20 mL of ethanol at about 75 °C and slowly added dropwise into the *l*PEI ethanol solution of equivolume under stirring. The solvent was slowly vaporized until a white solid appeared, which was separated by filtration, washed with ethanol, and dried under vacuum for 48 h at room temperature. The nitrogen content N (wt %) of the complex was determined with a Vario EL elemental analyzer, and the composition *x* was estimated and listed in Table 1. For preparing pyrene-doped complex film (containing pyrene of 0.05 wt %), to the THF solution of complexes was the THF solution of pyrene added, and the homogeneous solution was then coated on a quartz glass at room temperature and dried under vacuum at 60 °C.

Measurement. The Fourier transform infrared (FTIR) spectrum of all complexes was recorded on a Bruker Vector 33 FTIR spectrometer using KBr pellets at room temperature. Wide-angle X-ray diffraction (WAXD) and small-angle X-ray scattering (SAXS) measurements of the complex power were performed in transmission geometry with a X'pert PRO diffractometer (40 kV and 40 mA) using Cu Kα radiation (wavelength $\lambda = 0.154$ nm) at room temperature. The 2θ ranged from 10° to 30° for WAXD, and the scattering vector s ranged from 0.113 to 1.55 nm^{-1} for SAXS, where $s = (2/\lambda)\sin\theta$. The scan step was 0.01° in 2θ with a counting time of 2 s/step. The fluorescence emission spectrum of the pyrene-doped complex film on a quartz glass was observed using a Hitachi F-4500 fluorescence spectrophotometer with an excitation wavelength of 335 nm and slits of 5/5 nm at room temperature. The differential scanning calorimetry (DSC) experiment was performed with 3−5 mg of sample in a 6 mm aluminum pan on a Netzsch DSC 204 under a nitrogen atmosphere at a heating or cooling rate of 10 °C/min following the temperature sequence as room temperature → 140 °C → −60 °C → 140 °C. Thermogravimetry (TG) was measured with a Netzsch TG 209 under a nitrogen atmosphere at a heating rate of 10 °C/min starting from room temperature to 500 °C. A polarized optical microscope of Zeiss Axiophot was used with a Linkam hot stage. The sample was heated from room temperature to 140 °C and held for 3 min at 140 °C to remove the heat history and then cooled to room temperature and subsequently heated to 70 °C again at a rate of 10 °C/min. All the photos were taken at 70 °C.

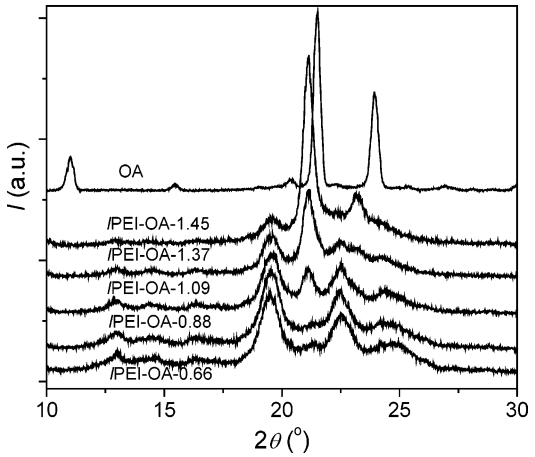

Figure 1. WAXD patterns of the complexes *l*PEI−OA-*x* at room temperature with indicated *x* value.

Table 2.. WAXD Space of *l*PEI−OA Complexes

sample	*d* (nm)				
*l*PEI−OA-0.66	0.46	0.42	0.39		0.36
*l*PEI−OA-0.88	0.46	0.42	0.39		0.36
*l*PEI−OA-1.09	0.46	0.42	0.39		0.36
*l*PEI−OA-1.37	0.46	0.42	0.39	0.38	0.36
*l*PEI−OA-1.45	0.46	0.42	0.39	0.38	0.36

Results and Discussion

Side-Chain Crystallization. WAXD was performed to reveal supramolecular structures of the complex. Figure 1 shows the WAXD profiles of the *l*PEI−OA complexes compared with that of pure OA. All complexes display sharp diffraction peaks within the 2θ range of 17°−28°, which indicates the crystalline structure of the bound OA alkyl tails. The *d*-space of the corresponding diffraction peaks is listed in Table 2. The diffraction positions (2θ) for all the complexes in Figure 1 are similar, but the diffraction intensity varies with the composition *x*. With increasing *x* from *l*PEI−OA-0.66 to *l*PEI−OA-1.45, the peaks at $d = 0.46$ and 0.39 nm become weaker and the peaks at $d = 0.42$ and 0.38 nm become stronger. These results mean that there should be a change in the packing structure of the side-chain crystals.

Before we are engaged in the interpretation of the structure change in our complexes, we simply introduce the crystal structure of *n*-paraffin with even *n* values larger than 24. There are β-orthorhombic (β_O) and

β-triclinic (β_T) modifications with diffractions of d = 0.42, 0.38 nm and d = 0.45, 0.38, 0.36 nm, respectively. Other modifications, such as α-hexagonal (α_H) with d = 0.42, 0.24, 0.21 nm and β-monoclinic (β_M) forms may also exist in the paraffin crystal.[14−16] For pure OA, two strong diffraction peaks are present at 2θ = 21.5° and 23.9° (correspondingly d = 0.41 and 0.37 nm) in its WAXD profile (Figure 1), indicating dominant β_O form in the pure OA crystal. There is more than one packing structure for the alkyl chains of bound OA molecules judging from the WAXD profiles in Figure 1 compared with the crystalline data of OA. For the samples *l*PEI−OA-1.45 and *l*PEI−OA-1.37 with higher OA content, the strong diffractions at 2θ = 21.1° and 23.2° (d = 0.42 and 0.38 nm) suggest that the β_O modification should be predominant in these complexes. At the same time, there are faint peaks at d-space of 0.46, 0.39, and 0.36 nm, corresponding to coexistence of the minor β_T crystalline modification. With decreasing x, the reflections at d-space of 0.42 and 0.38 nm significantly decrease and finally almost completely disappear when x below 0.88. In contrast, the reflection of d = 0.46 nm becomes predominant when x is below 1.09. The diffraction pattern of *l*PEI−OA-1.09 clearly indicates the coexistence of the β_O (d = 0.42 nm) and β_T (d = 0.46, 0.39, and 0.36 nm) modifications at this moderate composition. For *l*PEI−OA-0.88 and *l*PEI−OA-0.66, three main reflections at 2θ = 19.5°, 22.5°, and 24.6° correspond to d = 0.46, 0.39, and 0.36 nm from the β_T form of the alkyl chain crystal with a small part of β_O modification indicated by the faint diffraction at d = 0.42 nm. The above results indicate that the crystalline structure in *l*PEI−OA-x complexes is constituted by two modifications of β_O and β_T, and their proportion varies with the composition x. For the samples of $x > 1.0$, the β_O structure is dominant, while the β_T structure becomes dominant when $x < 1.0$. When $x \approx 1.0$ as the sample *l*PEI−OA-1.09, both β_O and β_T modifications are comparable in amount. For the complexes of $x > 1.0$, because OA molecules more than the number of amino groups in *l*PEI are included into the crystal, their alkyl chains are required to pack in parallel to each other and to align perpendicularly to the *l*PEI backbone for saving space. Thus, a denser packing structure with higher symmetry as β_O is favorable in forming the complex. As for $x < 1.0$, there are some charge sites of polymer free from binding OA. This will lead to a looser packing structure with lower symmetry as β_T.

Crystalline alkyl chain compounds are characterized by FTIR absorbance in the region centered at 720 cm^{-1} associated with the CH_2 rocking mode. The orthorhombic packing β_O of the hydrocarbon chains has dual absorbance bands at 719 and 727 cm^{-1}, while the triclinic β_T and hexagonal α_H structures have only one band at 717 and 720 cm^{-1}, respectively.[16] The FTIR spectra in Figure 2 depict two absorbance bands at 718 and 727 cm^{-1} for pure OA, confirming its β_O packing. For all the *l*PEI−OA-x complexes, there is a main band at about 720 cm^{-1} with a shoulder at about 728 cm^{-1}; the latter is gradually weakened with decreasing x. This FTIR observation also points out the structure change for the complex from β_T to β_O with increasing the bound OA on *l*PEI. However, we cannot ensure existence of the α_H modification at moderate x at present because its X-ray diffractions and FTIR absorbance bands always overlap with those of other modifications. While for *b*PEI−carboxylate complexes, Thünemann et al.[10] reported that partially crystalline alkyl tails formed the α_H structure because only a strong reflection with a Bragg spacing of 0.41 nm was found in the wide-angle scattering diagrams of the complexes at temperatures lower than melting point.

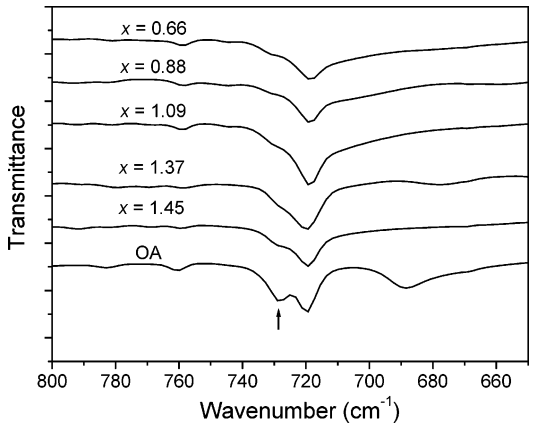

Figure 2. FTIR spectra of pure OA and *l*PEI−OA-x at room temperature with indicated x value.

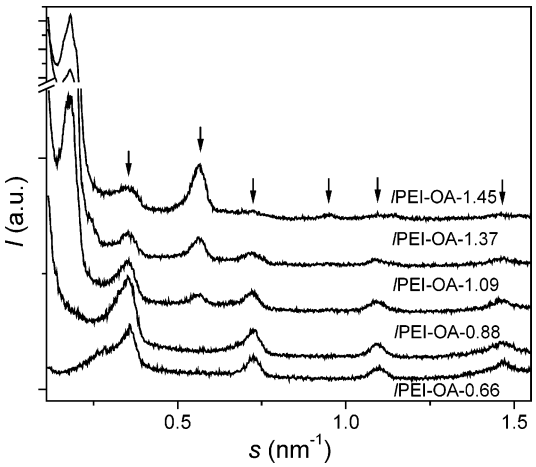

Figure 3. SAXS patterns of the complexes *l*PEI−OA-x at room temperature with indicated x valus. The arrows indicate the peak position.

Table 3. SAXS Space of *l*PEI−OA Complexes

sample	d (nm)						
*l*PEI−OA-0.66		2.77		1.38		0.907	0.682
*l*PEI−OA-0.88		2.84		1.37		0.913	0.681
*l*PEI−OA-1.09	5.58	2.84	1.76	1.38		0.915	0.682
*l*PEI−OA-1.37	5.56	2.84	1.76	1.40		0.918	0.685
*l*PEI−OA-1.45	5.53	2.84	1.77	1.38	1.05	0.914	0.690

Mesomorphous Structure. The SAXS patterns of the *l*PEI−OA-x complexes shown in Figure 3 illustrate at least four reflection peaks (indicated by the arrow) at equidistant position in s^{-1}, which is characteristic of a lamellar mesomorphous structure.[1,4] This lamella structure is known to consist of a n-alkyl chain crystalline layer of the bound OA aligning perpendicularly to the polyelectrolyte chain and an amorphous layer of polyelectrolyte chains with the polar heads of the amphiphile. The d-space of the corresponding scattering peaks is listed in Table 3. The observed long period is 2.77 nm for *l*PEI−OA-0.66, 2.84 nm for *l*PEI−OA-0.88, 5.58 nm for *l*PEI−OA-1.09, 5.57 nm for *l*PEI−OA-1.37, and 5.53 nm for *l*PEI−OA-1.45. The long period of *l*PEI−OA-0.66 and *l*PEI−OA-0.88 is larger than the length of fully extended alkyl chain of the OA molecule (2.4 nm[17]), indicating that the alkyl tails of OA in these

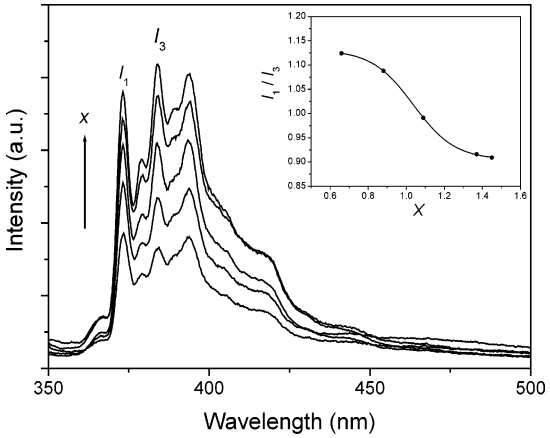

Figure 4. Fluorescence emission spectra of pyrene-doped complex films coated on a quartz glass as a function of x. Insert: plot of the I_1/I_3 values of pyrene in the complexes against x.

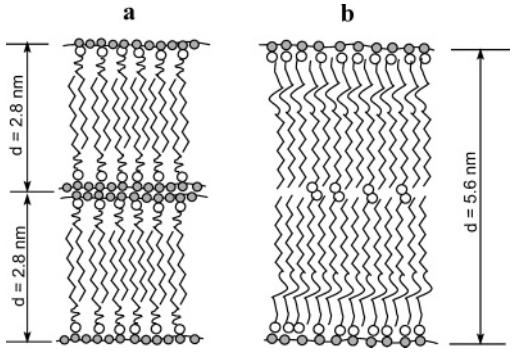

Figure 5. Schemes of two packing structures: (a) interdigitating monolayer model for $x < 1$ complexes; (b) end-to-end bilayer model for $x > 1$ complexes.

complexes of $x < 1.0$ are interdigitated and almost perpendicular to the *l*PEI chain. It is particularly worth noting that the long period ca. 5.6 nm of *l*PEI−OA-x with $x > 1.0$ is just twice of that for the complexes with $x < 1.0$, suggesting the formation of the end-to-end bilayer structure.

The steady-state fluorescence spectrum of the pyrene-doped complex films was measured to further understand packing of alkyl side chains in the lamellar structures. It is well-known that the monomer pyrene emits five fine bands between 370 and 400 nm, and the emission intensity ratio of the first to the third band I_1/I_3 can probe the microenvironment polarity around the pyrene moiety.[18] For example, the I_1/I_3 value is 0.58 in hexane and 1.87 in water.[19] As shown in Figure 4, the I_1/I_3 value of the complexes exhibits a rapid decrease from 1.12 to 0.91 with increasing x from 0.66 to 1.45, indicating a significant polarity decrease in the microenvironment around pyrene probes in the complexes. It is clear that the alkyl chains are arranged to form a more dense and less polar structure in the complexes of $x > 1.0$. This suggests that excess "free" OA molecules in the complexes of $x > 1.0$ would be incorporated into the crystalline layers of the OA alkyl tails to form a denser packing structure of β_O.

From the above results, we can conclude that there are two stacking structures for the bound surfactant molecules in the crystalline layer, as illustrated in Figure 5. One is formed by interdigitating alkyl tails pointing in opposite directions (interdigitating monolayer); the other is formed with the end groups to end

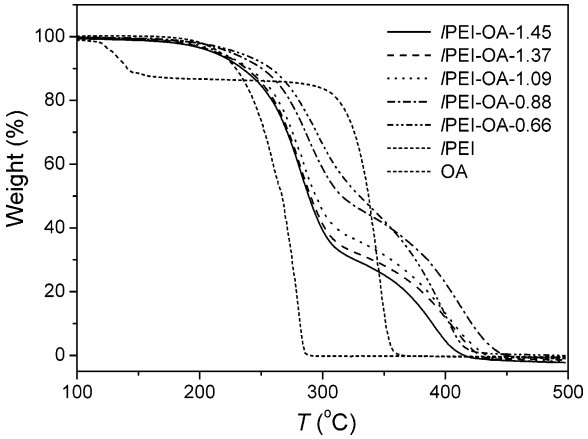

Figure 6. TG thermograms of pure OA, PEI, and *l*PEI−OA-x with $x = 0.66-1.45$.

groups (end-to-end bilayer). This means that the supramolecular structure of the complexes is transformed from the interdigitating monolayer to the end-to-end bilayer with the increase in the bound OA proportion. One may ask the binding force and packing structure for the case of $x > 1.0$ with the excess of OA molecules. In the end-to-end bilayer structure, the unbound or "free" OA molecules align parallel to the bound OA chains and cocrystallize together due to the hydrophobic interaction between their alkyl tails and hydrogen-bonding interaction between polar heads of OA molecules, causing a denser and more symmetric packing in the alkyl tail crystal as observed with WAXD.[9]

Thermal Properties. The thermal properties of the complexes were characterized using TG and DSC. TG thermograms of pure OA, PEI, and *l*PEI−OA-x ($x = 0.66-1.45$) are shown in Figure 6. All the complexes exhibit a two-step weight-loss process. The degradation temperature T_{d1} corresponding to the first maximum weight-loss rate is at 280−300 °C. This indicates that the thermal stability of the complexes is significantly raised by 30−50 °C compared with pure OA (255 °C) due to the strong electrostatic interaction between $-COO^-$ (from OA) and $=NH_2^+$ or $-NH_3^+$ (from *l*PEI). Furthermore, the second weight-loss step at 370−410 °C is attributed to the degradation of *l*PEI polymer in the complexes. The corresponding maximum degradation temperature T_{d2} significantly increases from 345 °C for pure *l*PEI to 375 and 410 °C for *l*PEI−OA-1.45 and *l*PEI−OA-0.88, respectively.

On the other hand, DSC traces plotted in Figure 7 indicate that there is no glass transition in all the complexes over the temperature range from −50 to 140 °C, consistent with that reported for *b*PEI−carboxylate complexes with different alkyl tails[12,13] due to the stiffening of the *l*PEI chains resulting from crystallization of the bound OA alkyl tails. Endothermic transitions have been observed from all the complexes during heating, which is due to melting of the OA alkyl tail crystal (melting temperature T_m of the β_O form is 67.7 °C). The double melting transition appears at ca. 58 and 66 °C for the *l*PEI−OA-x complexes of $x > 1.0$, corresponding to the melting of two crystalline modifications of β_T and β_O, respectively (Table 1), which coexist in these complexes as found with WAXD and FTIR. For the *l*PEI−OA-0.66 and *l*PEI−OA-0.88 complexes, only one main endothermic transition appears at ca. 58 °C (Table 1), indicating the predominant presence of the β_T form accompanied by a DSC-invisible β_O form.

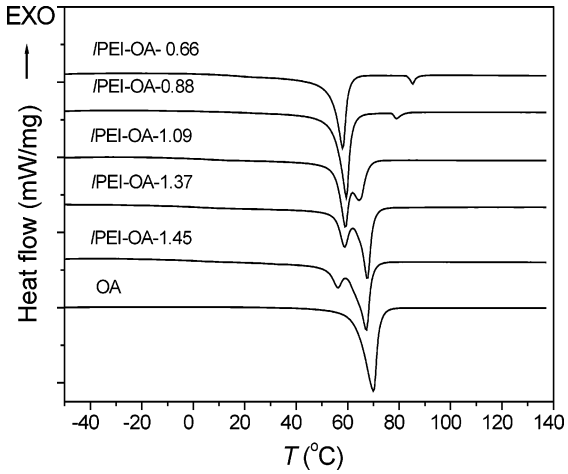

Figure 7. DSC traces of the complex *l*PEI−OA-*x* with indicated *x* values recorded during the second heating run at the rate of 10 °C/min.

To determine the amount of bound OA involved in the tail crystal, the transition heat ΔH_m evaluated from the DSC peak area (Table 1) is considered as the contribution only from the crystal melting of the bound OA tails. The decrease in ΔH_m also manifests the decrease of β_O form with decreasing *x*. The crystallinity of OA tails X_c^{OA} is estimated as

$$X_c^{OA} = \frac{\Delta H_m}{\Delta H_m^{OA} W_{OA}} \quad (1)$$

where W_{OA} is the OA weight fraction in the complex and ΔH_m^{OA} is the transition heat of pure OA. The ΔH_m values are within the range of 75.7−100.8 J/g for all the complexes, much smaller than 194 J/g for pure OA. Thus, the crystallinity X_c^{OA} of the bound OA tails is about 0.48−0.574 and slightly increased with increasing *x*, indicating an increased tendency of the OA tail crystal. The fact that the melting temperature of the complexes is lower than that of pure OA also testifies that the bound OA tail crystal is not as perfect as pure OA. The number of crystallized CH_2 groups in a OA chain, n_c, can be roughly estimated by using the relation $n_c = 17X_c^{OA}$. The calculated n_c values are listed in the rightmost column of Table 1. It is noted that only 8−10 CH_2 groups in an OA molecule participate in the crystallization, which is in good agreement with the crystalline characteristics of comb copolymers having long alkyl side chains.[20] The results suggest that the presence of several spacer CH_2 groups in a side chain would be necessary for the side-chain crystallization regardless of the bonding type, either covalent or ionic, between the side chain and the polymeric backbone.

Liquid-Crystalline State. Interestingly there is a weak endothermic transition at 78−85 °C in the DSC curve for *l*PEI−OA-0.66 and *l*PEI−OA-0.88 of $x < 1.0$. Both complexes exhibit birefringent fanlike textures under polarized light at 70 °C (Figure 8a,b), and the oriented texture can be observed after being sheared at 70 °C in one direction (Figure 8c,d). Therefore, these complexes are in a so-called thermotropic side-chain liquid crystalline state in the temperature range of ca. 58 °C (the main transition) to ~80 °C (the weak transition), although the pure OA never form liquid crystalline phase itself. The isotropic temperature T_i is 78.2 and 85.2 °C (peak value), and the corresponding

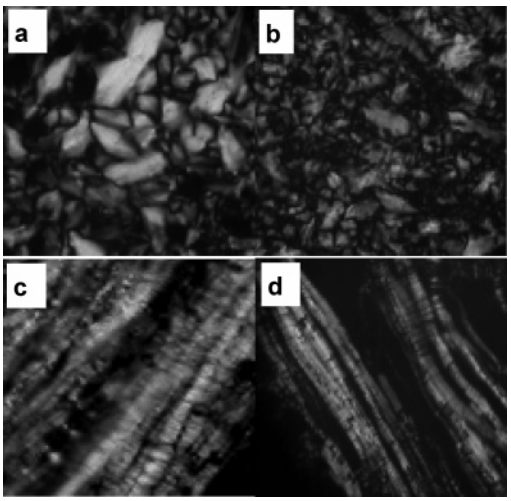

Figure 8. Polarized optical micrographs of the complexes at 70 °C: *l*PEI−OA-0.66 (a) and *l*PEI−OA-0.88 (b) before shearing; *l*PEI−OA-0.66 (c) and *l*PEI−OA-0.88 (d) after shearing.

transition heat is 3.03 J/g (0.86 kJ/mol) and 4.95 J/g (1.41 kJ/mol) for *l*PEI−OA-0.88 and *l*PEI−OA-0.66, respectively. These values are close to the isotropic heat of 1.3−3.6 kJ/mol usually observed from small molecule liquid crystals.[21] It is worth noting that the complexes of $x > 1.0$ exhibit two separated endothermic transitions at 55−70 °C, corresponding to the β_T and β_O crystal melting, respectively, but without the liquid crystal state at even higher temperatures. The more symmetric stacking of β_O form and higher crystallinity seems to encumber the appearance of the liquid crystal state in the complexes of $x > 1.0$.

Conclusion

In summary, the alkyl tails of OA bound on *l*PEI form the crystalline structure varying with the molar ratio *x* of OA to the repeat unit of *l*PEI. There are two crystalline modifications β_O and β_T coexisting in the *l*PEI−OA complexes, and only 8−10 CH_2 groups from one bound OA molecule enter the crystal. The OA tail crystal with amorphous *l*PEI forms the lamella mesomorphous structure. The complexes with $x > 1.0$ are predominant with β_O form and stacked into an end-to-end bilayer lamella with the long period of ~5.6 nm, while for the complexes of $x < 1.0$ the β_T form is dominantly stacked in the interdigitating monolayer structure with the long period of ~2.8 nm. The fluorescence emission of the pyrene-doped complex films suggests the formation of denser and less polar microenvironment in the complexes with increasing *x*. Interestingly, the thermotropic liquid crystal state has been found from the complexes of $x < 1.0$ at the temperature above the melting point of the OA tail crystal. This study demonstrates that the crystalline and mesomorphous structure of polyelectrolyte−amphiphile complexes can be effectively controlled by changing the relative amount of bound amphiphiles. In other words, the stacking structure of amphiphile molecules depends on the amount of added binding polyelectrolytes.

Acknowledgment. The financial support from the NSF of China (20374021 and 90303019), the Specialized Research Fund for the Doctoral Program of the Education Ministry (20020561014), and the NSF of Guangdong Province (015036) is gratefully acknowledged.

References and Notes

(1) Thünemann, A. F. *Prog. Polym. Sci.* **2002**, *27*, 1473.
(2) Chen, L.; Xu, S.; McBranch, D.; Whitten, D. *J. Am. Chem. Soc.* **2000**, *122*, 9302.
(3) Thünemann, A. F.; Ruppelt, D.; Schnablegger, H.; Blaul, J. *Macromolarcules* **2000**, *33*, 2124.
(4) Antonietti, M.; Conrad, J.; Thünemann, A. *Macromolarcules* **1994**, *27*, 6007.
(5) Ruokolainen, J.; Tanner, J.; ten Brinke, G.; Ikkala, O.; Torkkeli, M.; Serimaa, R. *Macromolecules* **1995**, *28*, 7779.
(6) Ikkala, O.; Brinke, G. T. *Science* **2002**, *295*, 2407.
(7) Faul, C. F. J.; Antonietti, M. *Adv. Mater.* **2003**, *15*, 673.
(8) Hwang, M.-J.; Kim, K. *Langmuir* **1999**, *15*, 3563.
(9) Ujiie, S.; Takagi, S.; Sato, M. *High Perform. Polym.* **1998**, *10*, 139.
(10) Thünemann, A. F.; General, S. *Langmuir* **2000**, *16*, 9634.
(11) Ren, B.; Tong, Z.; Liu, X.; Wang, C.; Zeng, F. *Langmuir* **2004**, *20*, 10737.
(12) Fujiwara, T.; Ritchie, K.; Murakoshi, H.; Kusumi, A. *J. Cell Biol.* **2002**, *157*, 1071.
(13) Murase, K.; Fujiwara, T.; Umemura, Y.; Suzuki, K.; Iino, R.; Yamashita, H.; Saito, M.; Murakoshi, H.; Ritchie, K.; Kusumi, A. *Biophys. J.* **2004**, *86*, 4075.
(14) Bazuin, C. G.; Brodin, C. *Macromolecules* **2004**, *37*, 9366.
(15) Lee, J. L.; Pearce, E. M.; Kwei, T. K. *Macromolecules* **1997**, *30*, 6877.
(16) Luyten, M. C.; Alberda van Ekenstein, G. O. R.; ten Brinke, G.; Ruokolainen, J.; Ikkala, O.; Torkkeli, M.; Serimaa, R. *Macromolecules* **1999**, *32*, 4404.
(17) Cai, Y.; Wang, D.; Hu, X.; Xu, Y.; Zhao, Y.; Wu, J.; Xu, D. *Macromol. Rapid Commun.* **2001**, *22*, 504.
(18) Winnik, F. M. *Chem. Rev.* **1993**, *93*, 587.
(19) Dong, D. C.; Winnik, M. A. *Photochem. Photobiol.* **1982**, *35*, 17.
(20) Watanabe, J.; Ono, H.; Uematsu, I.; Abe, A. *Macromolecules* **1985**, *18*, 2141.
(21) Gray, G. W.; Goodby, J. W. J. *Smectic Liquid Crystals*; Leonard Hill: Glasgow, 1984; p 21.

MA050647+